www.ietdl.org

Published in IET Communications
Received on 19th April 2010
Revised on 25th February 2011
doi: 10.1049/iet-com.2010.0305

ISSN 1751-8628

Dual-hop multi-input multi-output relay systems over spatially correlated Nakagami-*m* fading channels

K.P. Peppas[1] *C.K. Datsikas*[2] *N.C. Sagias*[3] *G.S. Tombras*[2]

[1]*Laboratory of Wireless Communications, Institute of Informatics and Telecommunications, National Centre for Scientific Research-Demokritos, Agia Paraskevi, Athens 15310, Greece*
[2]*Department of Electronics, Computers, Telecommunications and Control, Faculty of Physics, University of Athens, Panepistimiopolis, Zografou, Athens 15784, Greece*
[3]*Department of Telecommunications Science and Technology, School of Applied Sciences and Technology, University of Peloponnese, end of Karaiskaki Street, Tripoli 22100, Greece*
E-mail: nsagias@ieee.org

Abstract: The authors study the performance of a dual-hop plus a direct link multiple-input multiple-output (MIMO) wireless communication system using orthogonal space–time block codes. The system under consideration is based on the decode-and-forward relaying protocol and operates over spatially correlated Nakagami-*m* fading channels. The proposed analysis is generic enough to account for any MIMO correlation model either from measurements or having theoretical and analytical justification. Analytical expressions for the system end-to-end outage and average symbol error probability are obtained, while critical parameters of the MIMO channel are taken into consideration such as the angle of arrival, the antenna array configuration, the wavelength and non-isotropic scattering conditions. Various numerical and computer simulation results demonstrate the proposed mathematical analysis and the impact of the above parameters to the system performance.

1 Introduction

Multi-hop relaying communications have recently attracted significant interest as they are able to provide a broad and efficient coverage in various contemporary communication networks. In multi-hop transmission, several intermediate nodes act as relays forwarding data from source to destination. Many protocols that take advantage of the benefits of multi-hop transmission have been proposed, with the decode-and-forward (DF) one demonstrating a reasonable trade-off between implementation complexity and error rate performance [1]. On the other hand, multiple-input multiple-output (MIMO) communication systems have received considerable attention in the last years owing to their potential for providing significant capacity and performance enhancement over conventional single-input single-output (SISO) systems [2].

Very recently, the application of MIMO systems in conjunction with relaying protocols has become a topic of increasing interest, due to the fact that this combination enables the design of sophisticated and high performance communication systems. For example in [3], assuming independent Rayleigh fading channels, exact expressions have been derived for the outage probability (OP) of the end-to-end signal-to-noise ratio (SNR) over MIMO relay channels using space–time block codes (STBCs) and the DF relaying protocol. In [4], an error rate study has been presented for the end-to-end performance of dual-hop regenerative and non-regenerative wireless communication systems with orthogonal STBCs (OSTBCs). The impact of spatial correlation on the performance of amplify-and-forward MIMO relay channels has been investigated in [5], considering correlated Rayleigh fading channels. Also in [6], closed-form expressions for the OP and average symbol error probability (ASEP) have been extracted for dual-hop transmissions with DF relaying over independent and non-identically distributed Nakagami-*m* fading channels employing partial relay selection. In that work the relay hop are all equipped with one antenna element.

In this paper we provide an end-to-end performance analysis of MIMO dual-hop DF systems. In an effort to generalise the above-mentioned works, all nodes are employed with multiple-antennas using OSTBCs, while not necessarily identically distributed spatially correlated Nakagami-*m* fading channels are considered. The adopted channel model is generic enough to account for any correlation model, for example, a model extracted from field measurements or mathematical models available in the open technical literature. We assume that a direct link between the source and the destination also exists and that the signals received at destination from the source and the relays are combined using maximum-ratio combining (MRC). Our analysis includes the effects of various parameters of interest such as non-isotropic scattering around the user, antenna array configuration and the mean directions of the signal arrivals.

Next, the following notations are used: $\Gamma(\cdot)$ and $\Gamma(\cdot,\cdot)$ for the gamma and the upper incomplete gamma functions [7, Equation (8.350.2)], respectively, ${}_pF_q(\cdot)$ for the generalised hypergeometric function, $J_0(\cdot)$ for the zero-order Bessel function of the first kind, $I_0(\cdot)$ for the zero-order modified Bessel function of the first kind, $\Phi_2^{(K)}(\cdot)$ for the confluent

Lauricella hypergeometric function of K variables [8, Equation 10, p. 62], $F_D^{(n)}(\cdot)$ for the Lauricella multiple hypergeometric function of n variables [9, Equations (7.2.4.57) and (7.2.4.15)], $\mathbb{E}_X\langle\cdot\rangle$ for the expectation operator with respect to random variable X, $F_X(\cdot)$ and $\mathcal{M}_X(\cdot)$ for the cumulative distribution function (CDF) and the moments generating function (MGF) of X, respectively, $\Pr\{\cdot\}$ for the probability operator, $j=\sqrt{-1}$, $\mathrm{vec}(\cdot)$ for the vectorising operator that maps the elements of a given matrix into a column vector, $(\cdot)^{\mathrm{H}}$ for the Hermitian transpose, $(\cdot)^{\mathrm{T}}$ for the matrix transpose, $(\cdot)^*$ for complex conjugate, $\otimes$ for the matrix Kronecker product, $\odot$ for the matrix element-wise (Hadamard) product, $||\cdot||_F^2$ for the square Frobenius norm, $\Re\{\cdot\}$ for the real part, and $\mathbb{L}\{\cdot;\cdot;\cdot\}$ and $\mathbb{L}^{-1}\{\cdot;\cdot;\cdot\}$ for the direct and the inverse Laplace transforms, respectively.

2 System and channel model

We consider an MIMO dual-hop system where a source node $\boldsymbol{S}$ communicates with a destination node $\boldsymbol{D}$ both directly (path α) and via a relay node $\boldsymbol{R}$ (path β). The source and the destination are equipped with N_{S} and N_{D} antennas, respectively, whereas the relay is equipped with N_{R} antennas. The relay uses the DF protocol to forward the data received from the source to the destination.

2.1 Channel model

A narrowband channel model is assumed that is considered as frequency non-selective. We denote as $\boldsymbol{H}_0\in\mathbb{C}^{N_{\mathrm{D}}\times N_{\mathrm{S}}}$, $\boldsymbol{H}_1\in\mathbb{C}^{N_{\mathrm{R}}\times N_{\mathrm{S}}}$ and $\boldsymbol{H}_2\in\mathbb{C}^{N_{\mathrm{D}}\times N_{\mathrm{R}}}$ the $\boldsymbol{S}\xrightarrow{\alpha}\boldsymbol{D}$, $\boldsymbol{S}\xrightarrow{\beta}\boldsymbol{R}$ and $\boldsymbol{R}\xrightarrow{\beta}\boldsymbol{D}$ channels matrices, respectively. The (j,k)th envelope element of the ℓth hop ($\ell=0,\,1,\,2$) $r_{\ell_{jk}}=|\boldsymbol{H}_{\ell_{jk}}|$ is Nakagami-m distributed, with probability density function given by $f_{r_{\ell_{jk}}}(r)=2r^{2m_\ell-1}\exp(-r^2)/\Gamma(m_\ell)$, where $m_\ell\geq 1/2$ is the fading parameter and $\mathbb{E}\langle r_{\ell_{jk}}^2\rangle=m_\ell$. For each one of the three hops, the impact of spatial correlation can be captured by three corresponding positive definite covariance matrices $\boldsymbol{R}_{cc_\ell}$, defined as $\boldsymbol{R}_{cc_\ell}\triangleq\mathbb{E}_{\boldsymbol{H}_\ell}\langle\boldsymbol{h}_\ell\,\boldsymbol{h}_\ell^{\mathrm{H}}\rangle$, with $\boldsymbol{h}_\ell=\mathrm{vec}(\boldsymbol{H}_\ell)$.

Various correlation models have been proposed to capture the impact of MIMO spatial correlation. Representative examples are the Kronecker product model [10, 11] and the Weichselberger *et al.* model [12]. The Kronecker model is capable of modelling both narrowband and wideband channels, whereas the Weichselberger *et al.* model can be applied only to narrowband channels [13].

2.1.1 Kronecker correlation model: The Kronecker model requires knowledge of the transmitter and receiver correlations (hereafter one-sided correlations) and assumes that they are independent, and therefore can be treated separately. More specifically, for the $\boldsymbol{S}\xrightarrow{\alpha}\boldsymbol{D}$ hop, the correlation matrix is given by

$$\boldsymbol{R}_{cc_0}=\boldsymbol{R}_{S,\alpha}\otimes\boldsymbol{R}_{D,\alpha} \tag{1a}$$

with $\boldsymbol{R}_{S,\alpha}=\mathbb{E}_{H_0}\langle H_0^{\mathrm{T}}H_0^*\rangle\in\Re^{N_{\mathrm{S}}\times N_{\mathrm{S}}}$ and $\boldsymbol{R}_{D,\alpha}=\mathbb{E}_{H_0}\langle H_0H_0^{\mathrm{H}}\rangle\in\Re^{N_{\mathrm{D}}\times N_{\mathrm{D}}}$ being the source and destination one-sided correlation matrices of path α, respectively. Moreover, for the $\boldsymbol{S}\xrightarrow{\beta}\boldsymbol{R}$ and $\boldsymbol{R}\xrightarrow{\beta}\boldsymbol{D}$ hops

$$\boldsymbol{R}_{cc_1}=\boldsymbol{R}_{S,\beta}\otimes\boldsymbol{R}_{R_d,\beta} \tag{1b}$$

and

$$\boldsymbol{R}_{cc_2}=\boldsymbol{R}_{R_s,\beta}\otimes\boldsymbol{R}_{D,\beta} \tag{1c}$$

respectively, with $\boldsymbol{R}_{S,\beta}=\mathbb{E}_{H_1}\langle H_1^{\mathrm{T}}H_1^*\rangle\in\Re^{N_{\mathrm{S}}\times N_{\mathrm{S}}}$, $\boldsymbol{R}_{R_d,\beta}=\mathbb{E}_{H_1}\langle H_1H_1^{\mathrm{H}}\rangle\in\Re^{N_{\mathrm{R}}\times N_{\mathrm{R}}}$, $\boldsymbol{R}_{R_s,\beta}=\mathbb{E}_{H_2}\langle H_2^{\mathrm{T}}H_2^*\rangle\in\Re^{N_{\mathrm{R}}\times N_{\mathrm{R}}}$ and $\boldsymbol{R}_{D,\beta}=\mathbb{E}_{H_2}\langle H_2H_2^{\mathrm{H}}\rangle\in\Re^{N_{\mathrm{D}}\times N_{\mathrm{D}}}$ being the source, relay as receiver, relay as transmitter and destination one-sided correlation matrices of path β, respectively. Experiments have shown that the Kronecker structure describes quite well systems equipped with small number of antenna elements, for example, 2×2, however, it looses precision as the number of elements increases [13, 14]. Nevertheless, it remains by far the most popular MIMO channel model in the literature especially due to its simplicity.

2.1.2 Weichselberger et al. correlation model: The Weichselberger *et al.* model is slightly more complex than the Kronecker model, but has been shown to provide a better match in predicting a variety of channel metrics [12]. This model requires knowledge of source and destination one-sided correlation matrices, as in the Kronecker case, while additionally, requires knowledge of power coupling matrices, $\boldsymbol{\Omega}_\ell$s. By denoting the transmit and receive ends of the ℓth hop as $T_{x,\ell}$ and $R_{x,\ell}$, respectively, an estimate of $\boldsymbol{\Omega}_\ell$ can be obtained from the measured impulse response, $\boldsymbol{H}_\ell$, as

$$\boldsymbol{\Omega}_\ell=\mathbb{E}_{\boldsymbol{H}_\ell}\langle(\boldsymbol{U}_{R_{x,\ell}}^{\mathrm{H}}\boldsymbol{H}_\ell\boldsymbol{U}_{T_{x,\ell}}^*)\odot(\boldsymbol{U}_{R_{x,\ell}}^{\mathrm{T}}\boldsymbol{H}_\ell^*\boldsymbol{U}_{T_{x,\ell}})\rangle \tag{2}$$

where $\boldsymbol{U}_{R_{x,\ell}}$ and $\boldsymbol{U}_{T_{x,\ell}}$ are the eigenbases of one-sided correlation matrices at receive and transmit ends, respectively. The elements of this matrix, $\omega_{\ell_{i,j}}$s, denote the average power of the virtual SISO channel between the ith eigenmode of the transmit side and the jth eigenmode of the receive side of the ℓth hop. The correlation matrix for the $\boldsymbol{S}\xrightarrow{\alpha}\boldsymbol{D}$ hop is [12, Equation (6)]

$$\boldsymbol{R}_{cc_0}=\sum_{i=1}^{N_S}\sum_{j=1}^{N_D}\omega_{0_{i,j}}(\boldsymbol{u}_{\boldsymbol{S},\alpha,j}\otimes\boldsymbol{u}_{\boldsymbol{D},\alpha,i})(\boldsymbol{u}_{\boldsymbol{S},\alpha,j}\otimes\boldsymbol{u}_{\boldsymbol{D},\alpha,i})^{\mathrm{H}} \tag{3a}$$

where $\boldsymbol{u}_{\boldsymbol{S},\alpha,j}$ and $\boldsymbol{u}_{\boldsymbol{D},\alpha,i}$ are the jth and ith eigenvectors of the one-sided correlation matrices $\boldsymbol{R}_{S,\alpha}$ and $\boldsymbol{R}_{D,\alpha}$, respectively. Also, for the $\boldsymbol{S}\xrightarrow{\beta}\boldsymbol{R}$ and $\boldsymbol{R}\xrightarrow{\beta}\boldsymbol{D}$ hops

$$\boldsymbol{R}_{cc_1}=\sum_{i=1}^{N_S}\sum_{j=1}^{N_R}\omega_{1_{i,j}}(\boldsymbol{u}_{\boldsymbol{S},\beta,j}\otimes\boldsymbol{u}_{\boldsymbol{R}_d,\beta,i})(\boldsymbol{u}_{\boldsymbol{S},\beta,j}\otimes\boldsymbol{u}_{\boldsymbol{R}_d,\beta,i})^{\mathrm{H}} \tag{3b}$$

and

$$\boldsymbol{R}_{cc_2}=\sum_{i=1}^{N_R}\sum_{j=1}^{N_D}\omega_{2_{i,j}}(\boldsymbol{u}_{\boldsymbol{R}_s,\beta,j}\otimes\boldsymbol{u}_{\boldsymbol{D},\beta,i})(\boldsymbol{u}_{\boldsymbol{R}_s,\beta,j}\otimes\boldsymbol{u}_{\boldsymbol{D},\beta,i})^{\mathrm{H}} \tag{3c}$$

with $\boldsymbol{u}_{\boldsymbol{S},\beta,i}$, $\boldsymbol{u}_{\boldsymbol{R}_d,\beta,i}$, $\boldsymbol{u}_{\boldsymbol{R}_s,\beta,i}$ and $\boldsymbol{u}_{\boldsymbol{D},\beta,i}$ being the ith eigenvectors of correlation matrices $\boldsymbol{R}_{S,\beta}$, $\boldsymbol{R}_{R_d,\beta}$, $\boldsymbol{R}_{R_s,\beta}$ and $\boldsymbol{R}_{D,\beta}$, respectively.

2.1.3 One-sided correlation models: In general, the elements of the one-sided correlation matrices can be obtained from field measurements, for example, as in Section 2.1.1. Alternatively, various models can be used, such as the Abdi-Kaveh [15], exponential, constant and so on [16].

According to the Abdi-Kaveh model, the entries of the correlation matrix are

$$\varrho_{\boldsymbol{R}|_{jk}} = \frac{1}{I_0(\kappa)} I_0\left[\sqrt{\kappa^2 - 4\pi^2 \frac{d_{j,k}^2}{\lambda^2} + j4\pi\kappa \sin(\eta)\frac{d_{j,k}}{\lambda}}\right] \quad (4)$$

where $\eta \in [-\pi, \pi)$ is the mean direction of the angle of arrival (AOA), $\kappa \geq 0$ controls the width of the AOA ($\kappa = 0$ denotes isotropic scattering, whereas $\kappa = \infty$ stands for extremely non-isotropic scattering), λ denotes the wavelength and $d_{j,k}$ is the separation distance between the pair of receive antennas j and k. In the case of isotropic scattering around the user, (4) reduces to the Clarke's spatial correlation model $\varrho_{\boldsymbol{R}|_{jk}} = J_0(2\pi d_{j,k}/\lambda)$ [17]. Furthermore, for the exponential and the constant correlation models, $\varrho_{\boldsymbol{R}|_{jk}} = \rho^{|j-k|}$ and $\varrho_{\boldsymbol{R}|_{jk}} = \rho$, respectively, with $|\rho| \leq 1$.

2.2 System model

The overall communication from $\boldsymbol{S}$ to $\boldsymbol{D}$ is achieved in two time frames [18]. Each frame consists of L time slots during which a complex M-ary phase-shift keying (PSK) or quadrature amplitude modulation (QAM) symbol is encoded by a OSTBC having code matrix $\mathcal{H}_{N_S,\mathcal{R}_{c,1}} \in \mathbb{C}^{L\times N_S}$ (or simply $\mathcal{H}_{N_S}$ when $\mathcal{R}_{c,1} = 1$) and rate $\mathcal{R}_{c,1} = L/N_S$. For example, OSTBC matrices are $\mathcal{H}_2$, $\mathcal{H}_{3,3/4}$ and $\mathcal{H}_{4,3/4}$. $\mathcal{H}_2$ denotes the Alamouti OSTBC matrix, $\mathcal{H}_{3,3/4}$ and $\mathcal{H}_{4,3/4}$ are the $\mathcal{R}_{c,1} = 3/4$ rate OSTBC matrices for three and four transmit antennas, respectively. In the first frame, $\boldsymbol{S}$ sends a signal to $\boldsymbol{R}$ and $\boldsymbol{D}$, with the equivalent SISO received SNRs per symbol being

$$\gamma_{sd} = \frac{\bar{\gamma}_0}{m_0 N_S \mathcal{R}_{c,1}} \|\boldsymbol{H}_0\|_F^2 \quad (5a)$$

$$\gamma_{sr} = \frac{\bar{\gamma}_1}{m_1 N_S \mathcal{R}_{c,1}} \|\boldsymbol{H}_1\|_F^2 \quad (5b)$$

respectively, where $\bar{\gamma}_0$, $\bar{\gamma}_1$, are the corresponding average SNRs, characterising the path-losses on the considered hops. During the same time frame, the relay decodes the signal from the source. If γ_{sr} is above a specified SNR threshold γ_t, then the relay is assumed to be able to fully decode the source message. The destination terminal has to wait for the assistance of the relay during the second time frame. We denote as Ξ_r the state of the relay [3] that when $\gamma_{sr} \geq \gamma_t(M)$, $\Xi_r = 1$ and when $\gamma_{sr} < \gamma_t(M)$, $\Xi_r = 0$, with $\gamma_t(M)$ being the required SNR for the successful decoding of the source message, that depends on the employed modulation scheme. Note that $\gamma_t(M)$ increases with the number of constellation points M in order to maintain a given level of error rate performance. Therefore $\gamma_t(M)$ may be written as $\gamma_t(M) = \gamma_{\text{ref}}/\sin^2(\pi/M)$ and $\gamma_t(M) = \gamma_{\text{ref}}2(M-1)/3$ for M-PSK and M-QAM constellations, respectively, where γ_{ref} is a normalisation constant.

In the second time frame and according to the DF protocol, if the relay cannot correctly decode the signal, it remains idle; otherwise, it transmits the decoded signal, after re-encoding it, towards node $\boldsymbol{D}$ with the equivalent SISO instantaneous received SNR per symbol being

$$\gamma_{rd} = \frac{\bar{\gamma}_2}{m_2 N_R \mathcal{R}_{c,2}} \|\boldsymbol{H}_2\|_F^2 \quad (5c)$$

with $\bar{\gamma}_2$ being the corresponding average SNR and code rate $\mathcal{R}_{c,2} = L/N_R$.

The signals received in the destination node during the two time frames are combined using the MRC scheme. Therefore the equivalent SISO end-to-end SNR per symbol at node $\boldsymbol{D}$ is

$$\gamma_d = \gamma_{sd} + \Xi_r \gamma_{rd} \quad (6)$$

Based on the above equation, next, the statistics of γ_d is analysed.

3 Statistics of the end-to-end SNR

In this section, the statistical properties of the end-to-end SNR are studied in terms of the CDF and the MGF.

3.1 Cumulative distribution function

Based on (6), the CDF of γ_d can be expressed as [3, Equations (4) and (8)]

$$\begin{aligned} F_{\gamma_d}(\gamma) &= \Pr\{\gamma_d < \gamma | \Xi_r = 1\}\Pr\{\Xi_r = 1\} \\ &\quad + \Pr\{\gamma_d < \gamma | \Xi_r = 0\}\Pr\{\Xi_r = 0\} \\ &= F_{\gamma_{\text{mrc}}}(\gamma)[1 - F_{\gamma_{sr}}(\gamma_t(M))] + F_{\gamma_{sd}}(\gamma)F_{\gamma_{sr}}(\gamma_t(M)) \end{aligned} \quad (7)$$

with $\gamma_{\text{mrc}} = \gamma_{sd} + \gamma_{rd}$. The CDFs of γ_{sd}, γ_{sr}, γ_{rd} and γ_{mrc} appearing in (7) can be obtained from their corresponding MGFs using inverse Laplace transforms, that is, $F_x(\gamma) = \mathbb{L}^{-1}\{\mathcal{M}_x(s)/s; s; \gamma\}$. Using (5a), (5b) and [19, Equation (51)], these MGFs are given by

$$\mathcal{M}_{\gamma_{sd}}(s) = \prod_{k=1}^{K_0} (1 + s p_{0_k})^{-u_{0_k}} \quad (8a)$$

$$\mathcal{M}_{\gamma_{sr}}(s) = \prod_{k=1}^{K_1} (1 + s p_{1_k})^{-u_{1_k}} \quad (8b)$$

$$\mathcal{M}_{\gamma_{rd}}(s) = \prod_{k=1}^{K_2} (1 + s p_{2_k})^{-u_{2_k}} \quad (8c)$$

where $p_{0_k} = \lambda_k \bar{\gamma}_0/m_0 N_S \mathcal{R}_{c,1}$, $u_{0_k} = m_0\mu_k$, $p_{1_k} = \zeta_k \bar{\gamma}_1/m_1 N_S \mathcal{R}_{c,1}$, $u_{1_k} = m_1\eta_k$, $p_{2_k} = \xi_k \bar{\gamma}_2/m_2 N_R \mathcal{R}_{c,2}$ and $u_{2_k} = m_2\nu_k$. In (8), $\{\lambda_1, \lambda_2, \ldots, \lambda_{K_0}\}$ are the eigenvalues of $\boldsymbol{R}_{cc_0}$ with μ_k being their corresponding multiplicities with $\sum_{k=1}^{K_0} \mu_k = N_S N_D$, $\{\zeta_1, \zeta_2, \ldots, \zeta_{K_1}\}$ are the eigenvalues of $\boldsymbol{R}_{cc_1}$ with η_k being their corresponding multiplicities with $\sum_{k=1}^{K_1} \eta_k = N_S N_R$, and $\{\xi_1, \xi_2, \ldots, \xi_{K_2}\}$ are the eigenvalues of $\boldsymbol{R}_{cc_2}$ with μ_k being their corresponding multiplicities with $\sum_{k=1}^{K_2} \nu_k = N_D N_R$. Furthermore based on (8), the MGF of γ_{mrc} can be expressed as

$$\mathcal{M}_{\gamma_{\text{mrc}}}(s) = \mathcal{M}_{\gamma_{sd}}(s)\mathcal{M}_{\gamma_{rd}}(s) = \prod_{k=1}^{K_3} (1 + s p_{3_k})^{-u_{3_k}} \quad (9)$$

where $K_3 = K_0 + K_2$, $p_{3_k} = p_{0_k}$, if $k \leq K_0$ and $p_{3_k} = p_{2_{k-K_0}}$, if $k > K_0$. Furthermore, $u_{3_k} = u_{0_k}$ if $k \leq K_0$, or $u_{3_k} = u_{2_{k-K_0}}$ if $k > K_0$. Using the above MGF expressions, it can be easily verified that in order to obtain the CDFs of γ_{sd}, γ_{sr},

doi: 10.1049/iet-com.2010.0305

γ_{rd} and γ_{mrc}, inverse Laplace transforms

$$F_{\gamma_\ell}(\gamma) = \mathbb{L}^{-1}\left\{\frac{1}{s}\prod_{k=1}^{K_\ell}(1+sp_{\ell_k})^{-u_{\ell_k}}; s; \gamma\right\} \tag{10}$$

should be performed. For $\ell = 0$, 1 and 2, the CDF of γ_{sd}, γ_{sr} and γ_{rd} are denoted, respectively, whereas for $\ell = 3$, the CDF of γ_{mrc}. We may observe that each factor $(1+sp_{\ell_k})^{-u_{\ell_k}}$ in (10) is the MGF of a gamma-distributed random variable (RV) with parameters $1/p_{\ell_k}$ and u_{ℓ_k}. Hence, the product of K_ℓ such factors may be considered as the MGF of the sum of K_ℓ independent gamma RVs, each with parameters $1/p_{\ell_k}$ and u_{ℓ_k}. Then using [20, Equation (2)] and the definition of the incomplete gamma function, (10) can be expressed as

$$F_{\gamma_\ell}(\gamma_\ell) = \prod_{j=1}^{K_\ell}\left(\frac{p_{\ell_m}}{p_{\ell_j}}\right)^{u_{\ell_j}} \sum_{k=0}^{\infty}\delta_{\ell_k}\left[1 - \frac{\Gamma\left(k+\sum_{j=1}^{K_\ell}u_{\ell_j}, \gamma_\ell/p_{\ell_m}\right)}{\Gamma\left(k+\sum_{j=1}^{K_\ell}u_{\ell_j}\right)}\right] \tag{11}$$

where $p_{\ell_m} = \min\{p_{\ell_j}\}$, $j = 1, 2, \ldots, K_\ell$ and the coefficients δ_{ℓ_k} may be recursively obtained as

$$\delta_{\ell_{k+1}} = \frac{1}{k+1}\sum_{i=1}^{k+1}\left[\sum_{j=1}^{K_\ell}p_{\ell_j}\left(1-\frac{p_{\ell_m}}{p_{\ell_j}}\right)^i\right]\delta_{\ell_{k+1-i}}, \quad k = 0, 1, 2, \ldots \tag{12}$$

with $\delta_{\ell_0} = 1$. Two alternative expressions for $F_{\gamma_\ell}(\gamma)$ may be obtained using [21] as

$$\begin{aligned} F_{\gamma_\ell}(\gamma) &= \frac{1}{2} - \frac{1}{\pi}\int_0^\infty \frac{\sin\left[\sum_{j=1}^{K_\ell}u_{\ell_j}\arctan(tp_{\ell_j}) - t\gamma\right]}{t\prod_{j=1}^{K_\ell}(1+t^2p_{\ell_j}^2)^{u_{\ell_j}/2}}\,\mathrm{d}t \\ &= \frac{\prod_{j=1}^{K_\ell}(\gamma/p_{\ell_j})^{u_{\ell_j}}}{\Gamma\left(1+\sum_{j=1}^{K_\ell}u_{\ell_j}\right)}\Phi_2^{(K_\ell)} \\ &\quad \times\left(u_{\ell_1}, \ldots, u_{\ell_{K_\ell}}, 1+\sum_{j=1}^{K_\ell}u_{\ell_j}, -\frac{\gamma}{p_{\ell_1}}, \ldots, -\frac{\gamma}{p_{\ell_{K_\ell}}}\right) \end{aligned} \tag{13}$$

Note that the infinite series representation of $F_{\gamma_\ell}(\gamma)$ in (11) as well as the integral representation in (13) are much more convenient for accurate and efficient numerical evaluation than the exact closed-form solution involving confluent Lauricella functions. Now using (11) and (12), or (13), the CDF of γ_{sd}, γ_{sr} and γ_{mrc} appearing in (7) can be obtained, and henceforth, $F_{\gamma_d}(\gamma)$ may be readily extracted. Note that for uncorrelated Rayleigh fading channels ($m_\ell = 1$, $\lambda_k = \zeta_k = \xi_k = 1$) and using the identity $\Phi_2^{(K_\ell)}(1, \ldots, 1, 1+K_\ell, -z, \ldots, -z) = {}_1F_1(K_\ell, 1+K_\ell, -z) = \gamma(K_\ell, z)K_\ell/z^{K_\ell}$ [7, Equation (8.351.2)], (13) reduces to a previously known result [3, Equation (10)].

3.2 Moments generating function

The MGF of γ_d, defined as $M_{\gamma_d}(s) = \mathbb{E}\langle\exp(-s\gamma_d)\rangle$, can be directly obtained from (7) as $\mathcal{M}_{\gamma_d}(s) = s\,\mathbb{L}\{F_{\gamma_d}(\gamma); \gamma; s\}$, yielding

$$M_{\gamma_d}(s) = \mathcal{M}_{\gamma_{\text{mrc}}}(s)[1 - F_{\gamma_{sr}}(\gamma_t(M))] + \mathcal{M}_{\gamma_{sd}}(s)F_{\gamma_{sr}}(\gamma_t(M)) \tag{14}$$

Although the above expression is in a general form, by restricting $\sum_{j=1}^{K_\ell}u_{\ell_j}$ to integer values, next we present a corresponding expression which is simpler to handle. With the help of [7, Equation (8.352.7)], the incomplete gamma function in (11) may be expressed as a weighted sum of exponentials. Furthermore, using direct Laplace transforms [7, Equations (17.13.1) and (17.13.17)], $\mathcal{M}_{\gamma_d}(s)$ may be expressed as

$$\begin{aligned} \mathcal{M}_{\gamma_d}(s) &= [1 - F_{\gamma_{sr}}(\gamma_t(M))]\prod_{j=1}^{K_3}\left(\frac{p_{3_m}}{p_{3_j}}\right)^{u_{3_j}} \\ &\quad \times\sum_{k=0}^{\infty}\delta_{3_k}\left[1 - \sum_{l=1}^{k+\sum_{j=1}^{K_3}u_{3_j}-1}\frac{sp_{3_m}}{(sp_{3_m}+1)^{l+1}}\right] \\ &\quad + F_{\gamma_{sr}}(\gamma_t(M))\prod_{j=1}^{K_0}\left(\frac{p_{0_m}}{p_{0_j}}\right)^{u_{0_j}} \\ &\quad \times\sum_{k=0}^{\infty}\delta_{0_k}\left[1 - \sum_{l=1}^{k+\sum_{j=1}^{K_0}u_{0_j}-1}\frac{sp_{0_m}}{(sp_{0_m}+1)^{l+1}}\right] \end{aligned} \tag{15}$$

4 End-to-end performance analysis

Using the results of Section 3, analytical expressions for two performance metrics of interest are derived, namely the OP and the ASEP of M-PSK and M-QAM modulations.

4.1 Outage probability

An important measure of performance in fading channels is the OP, denoting the probability that the instantaneous end-to-end SNR falls below a specified threshold γ_t. Using (7) and (11), or (13), the end-to-end OP of the MIMO dual-hop system under consideration may be obtained as

$$P_{\text{out}}(\gamma_t) = F_{\gamma_d}(\gamma_t) \tag{16}$$

4.2 Average symbol error probability

To evaluate the ASEP performance of the considered MIMO dual-hop system, we follow the MGF-based approach for the error performance of digital communications systems over fading channels outlined in [16].

4.2.1 M-PSK: The ASEP of M-ary PSK signals is given by [16, Equation (5.78)]

$$\begin{aligned} P_{se} &= \frac{1}{\pi}\int_{\pi/2}^{\pi-\pi/M}\mathcal{M}_{\gamma_d}\left(\frac{g_{\text{psk}}}{\sin^2(\theta)}\right)\mathrm{d}\theta \\ &\quad + \frac{1}{\pi}\int_0^{\pi/2}\mathcal{M}_{\gamma_d}\left(\frac{g_{\text{psk}}}{\sin^2(\theta)}\right)\mathrm{d}\theta \end{aligned} \tag{17}$$

where $g_{\text{psk}} = \sin^2(\pi/M)$. Next, we consider two solutions for P_{se}. The first one is for arbitrary values of u_{ℓ_j}s, while the second one is when restricting $\sum_{j=1}^{K_\ell} u_{\ell_j}$ to integer values.

For arbitrary values of u_{ℓ_j}, by substituting (14) to (17), integrals of the form

$$\mathcal{F}_{\text{PSK},1} = \frac{1}{\pi}\int_{\pi/2}^{\pi-\pi/M} \prod_{k=1}^{K_\ell}\left(1+\frac{g_{\text{psk}}}{\sin^2(\theta)}p_{\ell_k}\right)^{-u_{\ell_k}} \mathrm{d}\theta \tag{18a}$$

and

$$\mathcal{F}_{\text{PSK},2} = \frac{1}{\pi}\int_{0}^{\pi/2} \prod_{k=1}^{K_\ell}\left(1+\frac{g_{\text{psk}}}{\sin^2(\theta)}p_{\ell_k}\right)^{-u_{\ell_k}} \mathrm{d}\theta \tag{18b}$$

need to be evaluated, with $\ell = 0, 1, 2$. For the integral $\mathcal{F}_{\text{PSK},1}$ by performing the change of variable $x = \cos^2(\theta)/\cos^2(\pi/M)$ and after some necessary manipulations, one obtains

$$\begin{aligned}
\mathcal{F}_{\text{PSK},1} &= \frac{\cos(\pi/M)}{2\pi}\int_0^1 \left(x - x^2\cos^2\left(\frac{\pi}{M}\right)\right)^{-1/2} \\
&\quad\times \prod_{k=1}^{K_\ell}\left(1+\frac{p_{\ell_k}g_{\text{psk}}}{1-x\cos^2(\pi/M)}\right)^{-u_{\ell_k}} \mathrm{d}x \\
&= \frac{1}{2\pi}\cos\left(\frac{\pi}{M}\right)\prod_{k=1}^{K_\ell}(1+g_{\text{psk}}p_{\ell_k})^{-u_{\ell_k}} \\
&\quad\times \int_0^1 x^{-1/2}\left(1-x\cos^2\left(\frac{\pi}{M}\right)\right)^{\sum_{k=1}^{K_\ell}u_{\ell_k}-1/2} \\
&\quad\times \prod_{k=1}^{K_\ell}\left(1-\frac{\cos^2(\pi/M)}{1+p_{\ell_k}g_{\text{psk}}}x\right)^{-u_{\ell_k}} \mathrm{d}x \\
&= \frac{1}{\pi}\prod_{k=1}^{K_\ell}(1+g_{\text{psk}}p_{\ell_k})^{-u_{\ell_k}}\cos\left(\frac{\pi}{M}\right) \\
&\quad\times F_D^{(K_\ell+1)}\left(\frac{1}{2}, \{u_{\ell_k}\}_{k=1}^{K_\ell}, \frac{1}{2}-\sum_{k=1}^{K_\ell}u_{\ell_k}; \frac{3}{2}; \right. \\
&\quad\times \left.\left\{\frac{\cos^2(\pi/M)}{1+g_{\text{psk}}p_{\ell_k}}\right\}_{k=1}^{K_\ell}, \cos^2\left(\frac{\pi}{M}\right)\right)
\end{aligned} \tag{19}$$

where $F_D^{(n)}(v, k_1, \ldots, k_n; c; z_1, \ldots, z_n)$ is the Lauricella multiple hypergeometric function of n variables defined as

$$\begin{aligned}
&F_D^{(n)}(v, k_1, \ldots, k_n; c; z_1, \ldots, z_n) \\
&\quad= \frac{\Gamma(c)}{\Gamma(c-v)\Gamma(v)}\int_0^1 x^{v-1}(1-x)^{c-v-1}\prod_{i=1}^{n}(1-z_i x)^{-k_i}\,\mathrm{d}x \\
&\quad= \sum_{l_1,l_2,\ldots,l_n=0}^{\infty}\frac{(v)_{l_T}}{(c)_{l_T}}\prod_{i=1}^{n}\frac{(k_i)_{l_i}}{\Gamma(l_i+1)}z_i^{l_i}, \quad z_i| < 1
\end{aligned} \tag{20}$$

where $l_T = \sum_{i=1}^{n} l_i$, $(\alpha)_\beta = \Gamma(\alpha+\beta)\ /\Gamma(\alpha)$ is the Pochhammer symbol. The integral in (20) exists when $\Re\{c-v\} > 0$ and $\Re\{v\} > 0$. It can be seen from (19) that the conditions for series convergence and integral existence of $F_D^{(K_\ell+1)}$ are satisfied. Note that the Lauricella function can be evaluated numerically in a computational-efficient manner using its integral representation with the help of any of the well-known popular mathematical software packages such as Maple or Mathematica.

For the integral $\mathcal{F}_{\text{PSK},2}$, by performing the change of variable $x = \cos^2(\theta)$ and after some manipulations, we obtain

$$\begin{aligned}
\mathcal{F}_{\text{PSK},2} &= \frac{1}{2\pi}\prod_{k=1}^{K_\ell}(1+g_{\text{psk}}p_{\ell_k})^{-u_{\ell_k}} \\
&\quad\times \int_0^1 x^{-(1/2)}(1-x)^{\sum_{k=1}^{K_\ell}u_{\ell_k}-(1/2)} \\
&\quad\times \prod_{k=1}^{K_\ell}\left(1-\frac{1}{1+p_{\ell_k}g_{\text{psk}}}x\right)^{-u_{\ell_k}} \mathrm{d}x \\
&= \frac{\Gamma\left((1/2)+\sum_{k=1}^{K_\ell}u_{\ell_k}\right)\prod_{k=1}^{K_\ell}(1+g_{\text{psk}}p_{\ell_k})^{-u_{\ell_k}}}{2\sqrt{\pi}\Gamma\left(1+\sum_{k=1}^{K_\ell}u_{\ell_k}\right)} \\
&\quad\times F_D^{(K_\ell)}\left(\frac{1}{2}, \{u_{\ell_k}\}_{k=1}^{K_\ell}; 1+\sum_{k=1}^{K_\ell}u_{\ell_k}; \left\{\frac{1}{1+g_{\text{psk}}p_{\ell_k}}\right\}_{k=1}^{K_\ell}\right)
\end{aligned} \tag{21}$$

By restricting $\sum_{j=1}^{K_\ell} u_{\ell_j}$ to integer values and substituting (15) to (17), integrals of the form

$$\mathcal{I}_1(k, A) = \frac{g_{\text{psk}}}{\pi}\int_0^{\pi/2}\frac{\sin^{2k-2}(\theta)}{(A\sin^2(\theta)+g_{\text{psk}})^k}\mathrm{d}\theta \tag{22a}$$

and

$$\mathcal{I}_2(k, A) = \frac{g_{\text{psk}}}{\pi}\int_{\pi/2}^{\pi-\pi/M}\frac{\sin^{2k-2}(\theta)}{(A\sin^2(\theta)+g_{\text{psk}})^k}\mathrm{d}\theta \tag{22b}$$

need to be evaluated, with $k \geq 1$ and $A > 0$. By substituting $\cos^2(\vartheta) = \omega$ and with the help of [7, Equations (9.111) and (9.121.1)], $\mathcal{I}_1(k, A)$ can be expressed as

$$\mathcal{I}_1(k, A) = \frac{\sqrt{g_{\text{psk}}}}{2\sqrt{\pi}}\frac{\Gamma(k-1/2)}{\Gamma(k)(A+g_{\text{psk}})^{k-1/2}} \tag{23}$$

Under the assumption of integer k, the integral in $\mathcal{I}_2(k, A)$ can be expressed in closed form as

$$\begin{aligned}
\mathcal{I}_2(k, A) &= \frac{(A+g_{\text{psk}})^{-k+1/2}}{\pi/\sqrt{g_{\text{psk}}}}\left[\frac{T_1}{2^{2k-2}}\binom{2k-2}{k-1}\right. \\
&\quad\left.+\frac{1}{2^{2k-3}}\sum_{j=0}^{k-2}\binom{2k-2}{j}\frac{\sin[(2k-2-2j)T_1]}{2k-2-2j}\right]
\end{aligned} \tag{24}$$

where $T_1 = \arccos[(A-\cos(2\pi/M))/(A+1)]/2$. In (24) and (30), when $2k-2j-2=0$, $\sin(2k-2j-2)/(2k-2j-2) = 1$. The proof of $\mathcal{I}_2(k, A)$ is given in Appendix.

doi: 10.1049/iet-com.2010.0305

4.2.2 Square M-QAM: The ASEP of square M-QAM constellations is given by

$$P_{se} = \frac{4\beta}{\pi}\int_0^{\pi/2} \mathcal{M}_{\gamma_d}\left(\frac{g_{\text{qam}}}{\sin^2(\vartheta)}\right) \mathrm{d}\vartheta - \frac{4\beta^2}{\pi}\int_0^{\pi/4} \mathcal{M}_{\gamma_d}\left(\frac{g_{\text{qam}}}{\sin^2(\vartheta)}\right) \mathrm{d}\vartheta \tag{25}$$

where $\beta = 1 - 1/\sqrt{M}$ and $g_{\text{qam}} = 3/[2(M-1)]$. Similar to M-PSK, next, we consider two solutions for P_{se}. The first one is for arbitrary values of u_{ℓ_j}s, whereas the second one is when restricting $\sum_{j=1}^{K_\ell} u_{\ell_j}$ to integer values.

For arbitrary values of u_{ℓ_j}, by substituting (14) to (25), integrals of the form

$$\mathcal{F}_{\text{QAM},1} = \frac{4\beta}{\pi}\int_0^{\pi/2} \prod_{k=1}^{K_\ell}\left(1 + \frac{g_{\text{qam}}}{\sin^2(\vartheta)} p_{\ell_k}\right)^{-u_{\ell_k}} \mathrm{d}\vartheta \tag{26a}$$

and

$$\mathcal{F}_{\text{QAM},2} = \frac{4\beta^2}{\pi}\int_0^{\pi/4} \prod_{k=1}^{K_\ell}\left(1 + \frac{g_{\text{qam}}}{\sin^2(\vartheta)} p_{\ell_k}\right)^{-u_{\ell_k}} \mathrm{d}\vartheta \tag{26b}$$

need to be evaluated, with $\ell = 0, 1, 2$. The first integral can be easily recognised to be similar to the one in the M-PSK case, and therefore it can be expressed as

$$\mathcal{F}_{\text{QAM},1} = \frac{2\beta\Gamma\left((1/2) + \sum_{k=1}^{K_\ell} u_{\ell_k}\right)\prod_{k=1}^{K_\ell}(1 + g_{\text{qam}} p_{\ell_k})^{-u_{\ell_k}}}{\sqrt{\pi}\Gamma\left(1 + \sum_{k=1}^{K_\ell} u_{\ell_k}\right)} \times F_D^{(K_\ell)}\left(\frac{1}{2}, \{u_{\ell_k}\}_{k=1}^{K_\ell}; 1 + \sum_{k=1}^{K_\ell} u_{\ell_k}; \left\{\frac{1}{1 + g_{\text{qam}} p_{\ell_k}}\right\}_{k=1}^{K_\ell}\right) \tag{27}$$

For the integral $\mathcal{F}_{\text{QAM},2}$, upon making the change of variable $x = 1 - \tan^2(\vartheta)$ and after some manipulations, we obtain

$$\begin{aligned}\mathcal{F}_{\text{QAM},2} &= \frac{4\beta^2}{\pi}\prod_{k=1}^{K_\ell}(1 + 2g_{\text{qam}}\, p_{\ell_k})^{-u_{\ell_k}} \int_0^1 (1-x)^{\sum^{K_\ell} u_{\ell_k} - (1/2)} \\ &\quad \times \prod_{k=1}^{K_\ell}\left(1 - \frac{1 + g_{\text{qam}}\, p_{\ell_k}}{1 + 2g_{\text{qam}}\, p_{\ell_k}} x\right)\left(1 - \frac{x}{2}\right)^{-1} \mathrm{d}x \\ &= \frac{\beta^2 \prod_{k=1}^{K_\ell}(1 + 2g_{\text{qam}}\, p_{\ell_k})^{-u_{\ell_k}}}{\pi(1/2 + \sum_{k=1}^{K_\ell} u_{\ell_k})} \\ &\quad \times F_D^{(K_\ell+1)}\left(1, \{u_{\ell_k}\}_{k=1}^{K_\ell}, 1; \right. \\ &\quad \left. \frac{3}{2} + \sum_{k=1}^{K_\ell} u_{\ell_k}; \left\{\frac{1 + g_{\text{qam}}\, p_{\ell_k}}{1 + 2g_{\text{qam}}\, p_{\ell_k}}\right\}_{k=1}^{K_\ell}, \frac{1}{2}\right)\end{aligned} \tag{28}$$

By restricting $\sum_{j=1}^{K_\ell} u_{\ell_j}$ to integer values and substituting (15) to (25), the first integral has a similar form to $I_1(k, A)$, that is

$$\begin{aligned}\mathcal{K}_1(k, A) &= \frac{4\beta g_{\text{qam}}}{\pi}\int_0^{\pi/2} \frac{\sin^{2k-2}(\theta)}{(A\sin^2(\theta) + g_{\text{qam}})^k} \mathrm{d}\theta \\ &= \frac{2\beta\sqrt{g_{\text{qam}}}}{\sqrt{\pi}} \frac{\Gamma(k - 1/2)/\Gamma(k)}{(A + g_{\text{qam}})^{k-1/2}}\end{aligned} \tag{29a}$$

while the second integral is

$$\mathcal{K}_2(k, A) = \frac{4\beta^2 g_{\text{qam}}}{\pi}\int_0^{\pi/4} \frac{\sin^{2k-2}(\theta)}{(A\sin^2(\theta) + g_{\text{qam}})^k} \mathrm{d}\theta \tag{29b}$$

Based on Appendix (Section 8.2) and under the assumption of integer k, the integral in $\mathcal{K}_2(k, A)$ can be expressed in closed form as

$$\mathcal{K}_2(k, A) = \frac{4\beta^2\sqrt{g_{\text{qam}}}}{\pi(A + g_{\text{qam}})^{k-1/2}}\left[\frac{T_2}{2^{2k-2}}\binom{2k-2}{k-1} + \frac{(-1)^{k-1}}{2^{2k-3}}\sum_{j=0}^{k-2}(-1)^j \binom{2k-2}{j} \frac{\sin[(2k-2-2j)T_2]}{2k-2-2j}\right] \tag{30}$$

where $T_2 = \pi/2 - \arccos(A/(A + 2g_{\text{qam}}))/2$.

4.2.3 Unified ASEP expression: Using the integral solutions of both Sections 4.2.1 and 4.2.2, a unified expression for the ASEP of both PSK and QAM when $\sum_{j=1}^{K_\ell} u_{\ell_j}$ is restricted to integer values can be written as

$$\begin{aligned}P_{se} &= [1 - F_{\gamma_{sr}}(\gamma_t(M))]\prod_{j=1}^{K_3}\left(\frac{p_{3_m}}{p_{3_j}}\right)^{u_{3_j}} \\ &\quad \times \sum_{k=0}^{\infty}\delta_{3_k}\left[1 - \frac{1}{M} - \sum_{l=1}^{k + \sum_{j=1}^{K_3} u_{3_j} - 1} p_{3_m}^{-l}\sum_{r=1}^{2}\mathcal{J}_r\left(l+1, \frac{1}{p_{3_m}}\right)\right] \\ &\quad + F_{\gamma_{sr}}(\gamma_t(M))\prod_{j=1}^{K_0}\left(\frac{p_{0_m}}{p_{0_j}}\right)^{u_{0_j}} \\ &\quad \times \sum_{k=0}^{\infty}\delta_{0_k}\left[1 - \frac{1}{M} - \sum_{l=1}^{k + \sum_{j=1}^{K_0} u_{0_j} - 1} p_{0_m}^{-l}\sum_{r=1}^{2}\mathcal{J}_r\left(l+1, \frac{1}{p_{0_m}}\right)\right]\end{aligned} \tag{31}$$

where for M-PSK $\mathcal{J}_i(k, A) \triangleq \mathcal{I}_i(k, A)$ and for M-QAM $\mathcal{J}_i(k, A) \triangleq \mathcal{K}_i(k, A)$, $i = 1, 2$.

4.3 Asymptotic end-to-end performance analysis

We observe that for $s \to \infty$, $\mathcal{M}_{\gamma_{sd}}(s)$ and $\mathcal{M}_{\gamma_{\text{mrc}}}(s)$ in (8) can be expressed as

$$\begin{aligned}\mathcal{M}_{\gamma_{sd}}(s) &= s^{-\sum_{k=1}^{K_0} u_{0_k}} \prod_{k=1}^{K_0} p_{0_k}^{-u_{0_k}} \prod_{k=1}^{K_0}\left(1 + \frac{1}{s p_{0_k}}\right)^{-u_{0_k}} \\ &= C_{sd} s^{-d_{sd}} + \mathcal{O}(s^{-d_{sd}})\end{aligned} \tag{32}$$

and

$$\mathcal{M}_{\gamma_{\mathrm{mrc}}}(s) = s^{-\sum_{k=1}^{K_3} u_{3_k}} \prod_{k=1}^{K_3} p_{3_k}^{-u_{3_k}} \prod_{k=1}^{K_3} \left(1 + \frac{1}{sp_{3_k}}\right)^{-u_{3_k}}$$
$$= C_{\mathrm{mrc}} s^{-d_{\mathrm{mrc}}} + \mathcal{O}(s^{-d_{\mathrm{mrc}}}) \quad (33)$$

where $C_{sd} = \prod_{k=1}^{K_0} p_{0_k}^{-u_{0_k}}$, $C_{\mathrm{mrc}} = \prod_{k=1}^{K_3} p_{3_k}^{-u_{3_k}}$, $d_{sd} = \sum_{k=1}^{K_0} u_{0_k}$ and $d_{\mathrm{mrc}} = \sum_{k=1}^{K_3} u_{2_k}$. We write $f(x) = \mathcal{O}[g(x)]$ as $x \to x_0$, if $\lim_{x \to x_0} (f(x)/g(x)) = 0$. Using [22, Proposition 3], it is obvious that d_{sd} is the diversity gain of the $\boldsymbol{S} \to \boldsymbol{D}$ hop, whereas d_{mrc} is the diversity gain for the combined $\boldsymbol{S} \to \boldsymbol{D}$ and $\boldsymbol{R} \to \boldsymbol{D}$ hop. The MGF of γ_d is then expressed as

$$M_{\gamma_d}(s) = [1 - F_{\gamma_{sr}}(\gamma_t(M))] C_{\mathrm{mrc}} s^{-d_{\mathrm{mrc}}} + F_{\gamma_{sr}}(\gamma_t(M)) C_{sd} s^{-d/sd} \quad (34)$$

Using (34) along with (17) and (25), simplified asymptotic expressions for the ASEP of M-PSK and M-QAM can be obtained. Also, the corresponding CDF can be easily obtained as

$$F_{\gamma_d}(\gamma) = [1 - F_{\gamma_{sr}}(\gamma_t(M))] C_{mrc} \frac{\gamma^{d_{\mathrm{mrc}}}}{\Gamma(d_{\mathrm{mrc}} + 1)} + F_{\gamma_{sr}}(\gamma_t(M)) C_{sd} \frac{\gamma^{d_{sd}}}{\Gamma(d_{sd} + 1)} \quad (35)$$

with the help of which and (16), an asymptotic expression for the end-to-end outage probability can be readily obtained.

5 Numerical and computer simulation results

In this section, we provide numerical and computer simulation results for the OP and ASEP performance of the considered dual-hop MIMO system. In order to show the generality of the presented results, the correlation models that are used are both analytical (see Section 2.1.3) as well from measurements.

We first consider a dual-hop system equipped with two antennas at the source, the relay and the destination nodes, where the Alamouti scheme is used. The impact of fading correlation is taken into account using the Kronecker model, where the transmit and receive correlation matrices at all hops ends are obtained using the Abdi-Kaveh model. Such a correlation has been derived under the assumption of a Rayleigh channel. However, the choice of a particular correlation structure is not an essential issue for the purpose of illustration. Since there is no alternative temporal correlation model available for Nakagami-m fading [23], next, we will use the Abdi-Kaveh correlation model in the following numerical examples. For the evaluation of the OP, a fixed M has been selected, so that $\gamma_t(M) = 0$ dB, whereas for the ASEP $\gamma_{\mathrm{ref}} = 0$ dB. Fig. 1 depicts the end-to-end OP using the Alamouti scheme against the first-hop normalised outage threshold, $\bar{\gamma}_1/\gamma_t$ for different values of the width of AOA, κ and as it is evident, the end-to-end OP improves as κ decreases. Furthermore, as expected, the balanced test case ($\bar{\gamma}_0 = \bar{\gamma}_1 = \bar{\gamma}_2$) outperforms the unbalanced one ($\bar{\gamma}_0 = \bar{\gamma}_2 = 0.5\bar{\gamma}_1$) for all the corresponding values of κ. For the same scenario, Table 1 shows the number of terms required in (11) to achieve an accuracy of up to the sixth-significant digit. As it is obvious, the infinite series converges rapidly and steadily requiring only a few terms for the target accuracy, especially at medium and high values of $\bar{\gamma}_1/\gamma_t$. Moreover, the number of required terms increases as κ increases and/or $\bar{\gamma}_1/\gamma_t$ decreases. For low values of $\bar{\gamma}_1/\gamma_t$, the integral representation in (13) may also be used to evaluate the OP. Fig. 2 depicts the end-to-end OP using the Alamouti

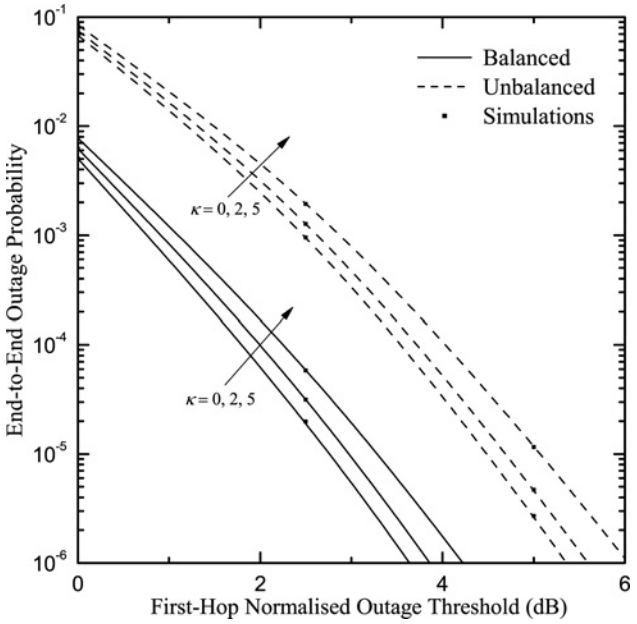

Fig. 1 *End-to-end OP of dual-hop DF MIMO relay system with orthogonal STBCs ($\mathcal{H}_2$ scheme), against first-hop normalised outage threshold under correlated Nakagami-m fading (Abdi-Kaveh model, uniform antenna arrays with $d_R = d_S = 10\lambda$, $\eta_S = \eta_R = \pi/4$, $d_D = 0.2\lambda$, $\eta_D = \pi/32$, $\kappa = 0, 2, 5$) $m_0 = 2.5$, $m_1 = m_2 = 1.5$, for unbalanced ($\bar{\gamma}_0 = \bar{\gamma}_2 = 0.5\bar{\gamma}_1$) and balanced ($\bar{\gamma}_0 = \bar{\gamma}_1 = \bar{\gamma}_2$) hops*

Table 1 Number of required terms for convergence of the outage probability based on (11) and (17) to achieve an accuracy of up to the sixth-significant digit (Abdi-Kaveh model, uniform antenna arrays with $d_R = d_S = 10\lambda$, $d_D = 0.2\lambda$, $\eta_S = \eta_R = \pi/4$, $\eta_D = \pi/32$, $\kappa = 0, 2, 5$, $m_0 = 2.5$, $m_1 = m_2 = 1.5$), for unbalanced hops ($\bar{\gamma}_0 = \bar{\gamma}_2 = 0.5\bar{\gamma}_1$)

$\bar{\gamma}_1/\gamma_t$, dB	$\kappa = 0$			$\kappa = 2$			$\kappa = 5$		
	$S \to D$	$S \to R$	MRC	$S \to D$	$S \to R$	MRC	$S \to D$	$S \to R$	MRC
0	47	7	40	63	6	58	110	6	104
2.5	27	3	20	38	4	29	68	3	58
5	16	2	8	22	4	13	38	2	25
7.5	7	2	3	11	2	6	20	2	14
10	3	2	2	3	2	3	9	1	7

doi: 10.1049/iet-com.2010.0305

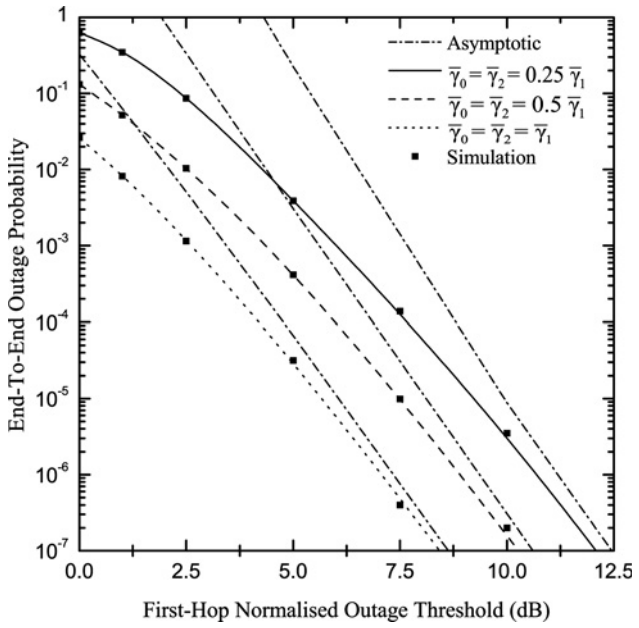

Fig. 2 *End-to-end OP of dual-hop DF MIMO relay system with orthogonal STBCs (2 transmit and receive antennas, $\mathcal{H}_2$ scheme), versus first-hop normalised outage threshold under correlated Nakagami-m fading (exponential correlation model, $\rho_S = 0$, $\rho_R = 0.1$, $\rho_D = 0.5$), $m_0 = 1.25$, $m_1 = 0.75$, $m_2 = 2.15$ for unbalanced ($\bar{\gamma}_0 = \bar{\gamma}_2 = 0.5\bar{\gamma}_1$, $\bar{\gamma}_0 = \bar{\gamma}_2 = 0.25\bar{\gamma}_1$), and balanced ($\bar{\gamma}_0 = \bar{\gamma}_1 = \bar{\gamma}_2$) hops*

scheme against $\bar{\gamma}_1/\gamma_t$ and its asymptotic behaviour for exponential correlation, balanced and unbalanced hops. As it can be observed, the asymptotic expression for the OP obtained using (35) correctly predicts the outage performance of the considered system at high values of $\bar{\gamma}_1/\gamma_t$, thus verifying the correctness of our analysis. In Fig. 3 the ASEP of M-ary PSK and square QAM is depicted as a function of $\bar{\gamma}_1$ for the Alamouti scheme, the Clarke correlation model and for different values of M. As shown, the ASEP always improves as $\bar{\gamma}_1$ increases and/or M decreases.

Next, we consider a dual-hop system equipped with four antennas at the source, the relay and the destination nodes, where the $\mathcal{H}_{4,3/4}$ code is used. We consider a more realistic propagation environment for the following two test cases. The first test case corresponds to the propagation environment presented in [24], where a narrowband Kronecker model was used, while the correlation matrices at both link ends were obtained from data collected in two types of environments, namely microcell and picocell. The term picocell and microcell refer to indoor-to-indoor and indoor-to-outdoor environment, respectively. In the picocell environment, the propagation scenario offers a decorrelated case, whereas in the microcell a correlated one. Note that although the Kronecker model generally performs poorly for MIMO systems equipped with more than two antennas, in this case, it agrees quite well with the measured data. The correlation matrices at the base station and the mobile terminal are [24, Equations (12) and 13)] (see (36a))

and (see (36b))

for picocell and (see (37a))

and (see (37b))

for microcell. Fig. 4 shows the end-to-end ASEP of the considered system when square M-QAM is employed for both considered environments under Rayleigh fading and for different values of M. As it can be observed, the error performance is slightly better in the picocell environment than in the microcell for all values of M. This result is in agreement with [24, Figure (12)], where the MIMO channel capacity of the picocell environment is better than the corresponding one of the microcell environment. The final test case is based on the experimental setup presented in [25]. Four-element single polarisation patches with half-wavelength spacing are considered, while the transmitter is fixed whereas the receiver can be at locations 2, 3 and 4. The Weichselberger *et al.* model has been adopted and based on measurements for $\boldsymbol{H}_\ell$s [26], the parameters of this

$$\boldsymbol{R}_{T_x,\text{pico}} = \begin{bmatrix} 1 & -0.45+0.53j & 0.37-0.22j & 0.19+0.21j \\ -0.45-0.53j & 1 & -0.35-0.02j & 0.02-0.27j \\ 0.37+0.22j & -0.35+0.02j & 1 & -0.10+0.54j \\ 0.19-0.21j & 0.02+0.27j & -0.10-0.54j & 1 \end{bmatrix} \tag{36a}$$

$$\boldsymbol{R}_{R_x,\text{pico}} = \begin{bmatrix} 1 & -0.13-0.62j & -0.49+0.23j & 0.15+0.28j \\ -0.13+0.62j & 1 & -0.13-0.52j & -0.38+0.12j \\ -0.49-0.23j & -0.13+0.52j & 1 & 0.02-0.61j \\ 0.15-0.28j & -0.38-0.12j & 0.02+0.61j & 1 \end{bmatrix} \tag{36b}$$

$$\boldsymbol{R}_{Tx,\text{micro}} = \begin{bmatrix} 1 & -0.61+0.77j & 0.14-0.94j & 0.24+0.89j \\ -0.61-0.77j & 1 & -0.85+0.50j & 0.57-0.78j \\ 0.14+0.94j & -0.85-0.50j & 1 & -0.91+0.40j \\ 0.24-0.89j & 0.57+0.78j & -0.91-0.40j & 1 \end{bmatrix} \tag{37a}$$

$$\boldsymbol{R}_{Rx,\text{micro}} = \begin{bmatrix} 1 & -0.12-0.18j & 0.08+0.05j & -0.02-0.13j \\ -0.12+0.18j & 1 & -0.17-0.16j & 0.11+0.04j \\ 0.08-0.05j & -0.17+0.16j & 1 & -0.17-0.16j \\ -0.02+0.13j & 0.11-0.04j & -0.17+0.16j & 1 \end{bmatrix} \tag{37b}$$

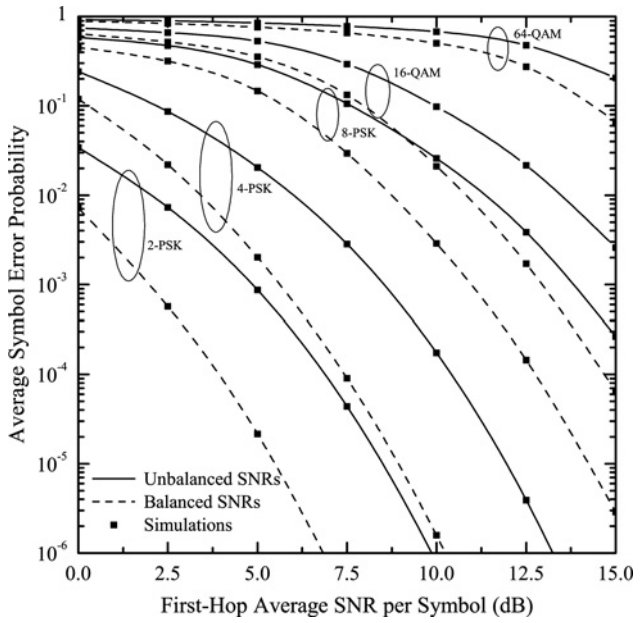

Fig. 3 *ASEP of M-ary PSK and M-ary QAM constellations of dual-hop DF MIMO relay systems with orthogonal STBCs (2 transmit and receive antennas, $\mathcal{H}_2$ scheme) against transmit SNR per symbol of the first hop, under correlated Nakagami-m fading (Clarke model, uniform antenna arrays with $d_R = d_S = 10\lambda$, $d_D = 0.2\lambda$), $m_0 = 2.5$, $m_1 = m_2 = 1.5$, for unbalanced ($\bar{\gamma}_0 = \bar{\gamma}_2 = 0.5\bar{\gamma}_1$) hops*

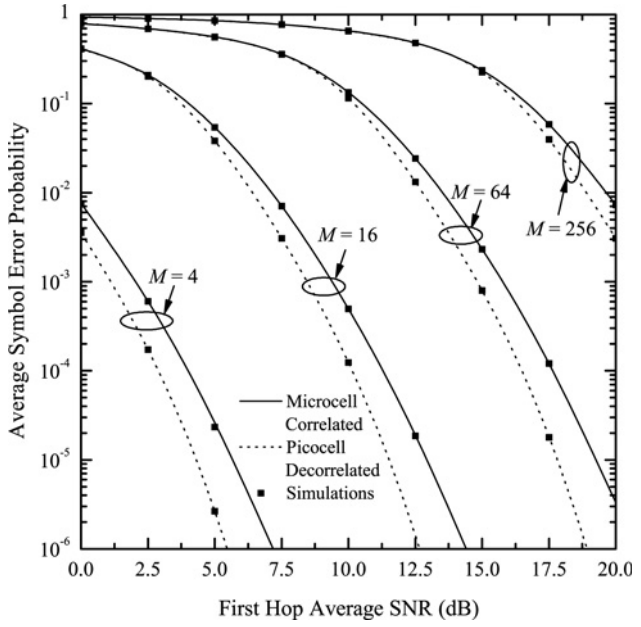

Fig. 4 *ASEP of M-ary QAM constellations of dual-hop DF MIMO relay systems with orthogonal STBCs (4 transmit and receive antennas, $\mathcal{H}_{4,3/4}$ scheme) against transmit SNR per symbol of the first hop, under correlated Rayleigh fading (picocell decorrelated and microcell correlated environments based on [24] for balanced hops ($\bar{\gamma}_0 = \bar{\gamma}_2 = \bar{\gamma}_1$)*

model can be easily extracted. More specifically, based on [26], we first performed an estimation of coupling matrices $\boldsymbol{\Omega}_\ell$s using (2) assuming that for a specific indoor location, a reasonable assumption is $R_{cc0} = R_{cc1} = R_{cc2}$. Then, the correlation matrices were estimated using (3). Furthermore, according to the findings of all experiments performed in

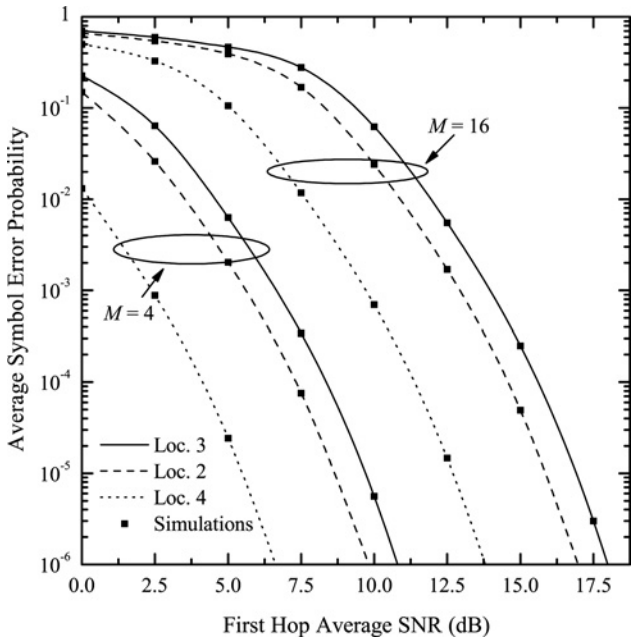

Fig. 5 *ASEP of M-ary QAM constellations of dual-hop DF MIMO relay systems with orthogonal STBCs (4 transmit and receive antennas, $\mathcal{H}_{4,3/4}$ scheme) against transmit SNR per symbol of the first hop, under correlated Rayleigh fading (Weicshelberger et al. model, based on the experimental setup in [25]) for balanced hops ($\bar{\gamma}_0 = \bar{\gamma}_2 = \bar{\gamma}_1$)*

[25], Rayleigh distributed channel envelopes were assumed for all considered hops. To demonstrate our analysis, Fig. 5 shows the ASEP of 4- and 16-QAM over Rayleigh fading as a function of $\bar{\gamma}_1$ in locations 2, 3 and 4, and as it is evident, ASEP improves as $\bar{\gamma}_1$ increases.

To verify the correctness of the proposed analysis, our numerically evaluated results are accompanied with semi-analytical Monte-Carlo simulations, where in our simulations, we form (6) with more than 10^7 samples. Note that the Frobenius norms involved in (5) are sums of correlated gamma variates. Hence, we can reduce the computational effort by using the fact that the sum of correlated gamma variates can be expressed as the sum of independent gamma variates with suitably scaled parameters, which depend on the elements of the covariance matrix. This result was first proved in [27], where the Karhunen-Loeve expansion was used to decorrelate arbitrarily correlated, non-identical, Erlang distributed RVs. Standard built-in functions available in popular mathematical software packages, such as the Matlab gamrnd function, can be readily used to generate gamma distributed samples with suitably defined parameters. Therefore, in Figs. 1–5, corresponding results are included (square signs) for comparison purposes. It can be observed that for all curves, we have an excellent match with the analytically evaluated results, validating the mathematical formulation.

6 Conclusions

A performance study of a DF dual-hop wireless communication system, employing OSTBC and operating over spatially correlated Nakagami-*m* fading channels was presented. Analytical expressions for the CDF and MGF of the end-to-end SNR were derived, valid for any orthogonal design and correlation model. Based on these formulas, a thorough performance analysis of the considered system was presented in terms of OP and ASEP of *M*-ary

doi: 10.1049/iet-com.2010.0305

modulation schemes. Extensive numerical and computer simulation results were presented that demonstrate the proposed mathematical analysis.

7 References

1 Laneman, J.N., Tse, D.N.C., Wornell, G.W.: 'Cooperative diversity in wireless networks: efficient protocols and outage behavior', *IEEE Trans. Inf. Theory*, 2004, **50**, (12), pp. 3062–3080
2 Paulraj, A., Nabar, R., Gore, D.: 'Introduction to space-time wireless communications' (Cambridge University Press, UK, 2003)
3 Chalise, B.K., Vandendorpe, L.: 'Outage probability analysis of a MIMO relay channel with orthogonal space-time block codes', *IEEE Trans. Commun.*, 2008, **12**, (4), pp. 280–282
4 Lee, I.H., Kim, D.: 'End-to-end BER analysis for dual-hop OSTBC transmissions over Rayleigh fading channels', *IEEE Trans. Commun.*, 2008, **56**, (3), pp. 347–351
5 Wagner, J., Rankov, B., Wittneben, A.: 'Large-*n* analysis of amplify-and forward MIMO relay channels with correlated Rayleigh fading', *IEEE Trans. Inf. Theory*, 2008, **54**, (12), pp. 5735–5746
6 da Costa, D.B., Aïssa, S.: 'Dual-hop decode-and-forward relaying systems with relay selection and maximal-ratio schemes', *Electron. Lett.*, 2009, **45**, (9), pp. 460–461
7 Gradshteyn, I.S., Ryzhik, I.M.: 'Tables of integrals, series, and products' (Academic Press, New York, 2000, 6th edn.)
8 Srivastava, H.M., Manocha, H.L.: 'A treatise on generating functions' (Wiley, New York, 1984)
9 Prudnikov, A.P., Brychkov, Y.A., Marichev, O.I.: 'Integrals and series volume 3: more special functions' (Taylor and Francis Ltd, 1998, 1st edn.)
10 Shiu, D.S., Foscini, G.J., Gans, M.J., Khan, J.M.: 'Fading correlation and its effect on the capacity of multielement antenna systems', *IEEE Trans. Commun.*, 2000, **48**, (3), pp. 502–513
11 Kim, I.M.: 'Exact BER analysis of OSTBCs in spatially correlated MIMO channels', *IEEE Trans. Commun.*, 2006, **54**, (8), pp. 1365–1373
12 Weichselberger, W., Herdin, M., Ozcelik, H., Bonek, E.: 'A stochastic MIMO channel model with joint correlation at both link ends', *IEEE Trans. Wirel. Commun.*, 2006, **5**, (1), pp. 90–100
13 Costa, N., Haykin, S.: 'Multiple-input multiple-output channel models: theory and practice' (Wiley, New Jersey, 2010)
14 Svantesson, T., Wallace, J.W.: 'Tests for assessing multivariate normality and the covariance structure of MIMO data'. Proc. IEEE Int. Conf. on Acoustics, Speech, and Signal Processing, 2003, vol. 4, pp. 656–659
15 Abdi, A., Kaveh, M.: 'A space–time correlation model for multielement antenna systems in mobile fading channels', *J. Sel. Areas Commun.*, 2002, **10**, (3), pp. 550–560
16 Simon, M.K., Alouini, M.S.: 'Digital communication over fading channels' (Wiley, New York, 2005, 2nd edn.)
17 Jakes, W.C.: 'Microwave mobile communications' (Wiley, New York, 1974)
18 Avestimehr, A.S., Tse, D.N.C.: 'Outage capacity of the fading relay channel in the low SNR regime', *IEEE Trans. Inf. Theory*, 2007, **53**, (4), pp. 1401–1415
19 Maaref, A., Aissa, S.: 'Performance analysis of orthogonal space–time block codes in spatially correlated MIMO Nakagami fading channels', *IEEE Trans. Wirel. Commun.*, 2006, **5**, (4), pp. 802–816
20 Alouini, M.S., Abdi, A., Kaveh, M.: 'Sum of gamma variates and performance of wireless communication systems over Nakagami-fading channels', *IEEE Trans. Veh. Technol.*, 2001, **50**, (6), pp. 1471–1480
21 Efthymoglou, G.P., Piboongungon, T., Aalo, V.A.: 'Performance analysis of coherent DS-CDMA systems in a Nakagami fading channel with arbitrary parameters', *IEEE Trans. Veh. Technol.*, 2006, **55**, (1), pp. 104–114
22 Wang, Z., Giannakis, G.: 'A simple and general parametrization quantifying performance in fading channels', *IEEE Trans. Commun.*, 2003, **51**, (8), pp. 1389–1398
23 Zhang, Q.T.: 'A decomposition technique for efficient generation of correlated Nakagami fading channels', *IEEE J. Sel. Areas Commun.*, 2000, **18**, (11), pp. 2385–2392
24 Kermoal, J.P., Schumacher, L., Pedersen, K.I., Mogensen, P.E., Frederiksen, F.: 'A stochastic MIMO radio channel model with experimental validation', *IEEE J. Sel. Areas Commun.*, 2002, **20**, (6), pp. 1211–1226
25 Wallace, J.W., Jensen, M.A., Swindlehurst, A.L., Jeffs, B.D.: 'Experimental characterization of the MIMO wireless channel: data acquisition and analysis', *IEEE Trans. Wirel. Commun.*, 2003, **2**, (2), pp. 335–343
26 Narrowband MIMO Measurement Platform.: http://wireless.groups.et.byu.net/research/probe/narrow_band/index.html
27 Win, M.Z., Chrisikos, G., Winters, J.H.: 'MRC performance for *M*-ary modulation in arbitrarily correlated Nakagami fading channels', *IEEE Commun. Lett.*, 2000, **4**, (10), pp. 301–303

8 Appendix

8.1 Evaluation of $\mathcal{I}_2(k, A)$

We first employ the change of variables $\theta = \phi - \pi/2$ in $\mathcal{I}_2(k, A)$ yielding

$$\mathcal{I}_2(k, A) = \frac{g_{\text{psk}}}{A^k \pi} \int_0^{\pi/2-\pi/M} \frac{\cos^{2k-2}(\theta)}{(\cos^2(\theta) + g_{\text{psk}}/A)^k} \, \mathrm{d}\theta$$
$$= \frac{g_{\text{psk}}}{(A + 2g_{\text{psk}})^k \pi} \int_0^{\pi-2\pi/M} \frac{(1 + \cos(\xi))^{k-1}}{(1 + d\cos(\xi))^k} \, \mathrm{d}\xi \tag{38}$$

where $d \triangleq A/(A + 2g_{\text{psk}})$. By employing the Euler–Legendre change of variables $\{1 + d\cos(\xi) = (1 - d^2)/(1 - d\cos(x)), \, \mathrm{d}\xi = \sqrt{1 - d^2}/(1 - d\cos(x))\,\mathrm{d}x\}$ and after some algebraic manipulations, the following form is obtained $\mathcal{I}_2(k, A) = g_{\text{psk}}/((A+2g_{\text{psk}})^k \pi)((1+d)^{1/2-k})/\sqrt{1-d} \int_0^{2T_1} (1+\cos(x))^{k-1} \, \mathrm{d}x$, where $2T_1 = \arccos[(A - \cos(2\pi/M)))/(A + 1)]$. By performing the change of variables $x = 2t$ and after some algebraic and trigonometric manipulations, $\mathcal{I}_2(k, A)$ can be expressed as

$$\mathcal{I}_2(k, A) = \frac{\sqrt{g_{\text{psk}}}}{\pi} (A + g_{\text{psk}})^{-k+1/2} \int_0^{T_1} \cos^{2k-2}(t) \, \mathrm{d}t \tag{39}$$

where using [7, Equation (2.513.3)], (24) is obtained.

8.2 Evaluation of $\mathcal{K}_2(k, A)$

After some algebraic and trigonometric manipulations, $\mathcal{K}_2(k, A)$ can be expressed as $\mathcal{K}_2(k, A) = 4\beta^2 \, g_{\text{qam}}/(\pi(A + g_{\text{qam}})^k) \int_0^{\pi/2} ((1 - \cos(\xi))^{k-1})/((1 - d\cos(\xi))^k) \mathrm{d}\xi$ where $d \triangleq A/(A + 2g_{\text{qam}})$. Similarly to Section 8.1, using the Euler–Legendre change of variables, the following form is obtained

$$\mathcal{K}_2(k, A) = (4\beta^2/\pi)(A + g_{\text{qam}})^{1/2-k} \sqrt{g_{\text{qam}}} \int_0^{T_2} \sin^{2k-2}(x) \mathrm{d}x \tag{40}$$

where $T_2 = \pi/2 - \arccos(A/(A + 2g_{\text{qam}}))/2$, while further using [7, Equation (2.513.1)], (30) is obtained.